Impact of nuclear reactions on gravitational waves from neutron star mergers

P. Hammond[*], I. Hawke, and N. Andersson

Mathematical Sciences and STAG Research Centre, University of Southampton,
Southampton SO17 1BJ, United Kingdom

Nuclear reactions may affect gravitational-wave signals from neutron-star mergers, but the impact is uncertain. To indicate the significance of this effect, we compare two numerical simulations representing intuitive extremes. In one case, reactions happen instantaneously. In the other case, they occur on timescales much slower than the evolutionary timescale. We show that, while the differences in the two gravitational-wave signals are small, the mismatch between them satisfies the condition for distinguishability using the Einstein Telescope noise curve, assuming that the neutron-star equation of state can be well constrained by experiments or by the postmerger signal of the event. This suggests that, to avoid systematic errors in equation of state parameters inferred from observed signals, we need to accurately implement nuclear reactions in future simulations.

I. INTRODUCTION

Binary neutron-star mergers are promising cosmic laboratories for extreme physics. As demonstrated in the celebrated case of GW170817 [1], one can use observed gravitational-wave merger signals (along with any electromagnetic counterparts) to make progress on the vexing issue of the state of matter at densities beyond nuclear. This motivates much of the current effort to develop robust numerical simulation technology (in full general relativity) to model these events [2,3], including as much realistic physics as possible. Reliable numerical relativity (and general relativistic magnetohydrodynamics) simulations are required to model the highly nonlinear dynamics at play and produce the signal templates needed for parameter extraction. In parallel, we need to improve the detector technology. The gravitational-wave signal from a merger event is characterized by frequencies above 1 kHz, where current ground-based instruments lose sensitivity.

While current interferometers could possibly detect the postmerger gravitational-wave signal from a nearby event, one would have to be very lucky for such an event to take place; with the spectacular GW170817 observation we may have been as fortunate as we are going to get, and in that case we did not observe the postmerger dynamics. In order to make our own luck, we need to push the development of third-generation instruments (like the Einstein Telescope [4–6] and the Cosmic Explorer [7,8]), which will have the potential to regularly catch neutron-star mergers [9].

At the same time, we need to make progress on the issue of extracting the physics we want to explore from observations. Motivated by this, simulations of large sets of mergers involving different matter equations of state (and physics implementations) have been carried out [10]. The results demonstrate how one may, indeed, expect to be able to distinguish different matter descriptions. This is promising, but a few points of caution are in order. In particular, we need to keep in mind that current simulations are not yet able to represent all aspects of the expected reality. Given the level of difficulty of the issues involved (especially concerning equilibrium [11] and neutrinos [12–16]), progress is slow. As we improve our simulations, we need to ensure that the results are sufficiently accurate and that the signal templates do not introduce systematic errors due to un- or underresolved physics. We will use the linked concepts of "mismatch" and "distinguishability" from gravitational-wave data analysis. The mismatch, quantified in Sec. II B, gives a criterion for when a given detector can observationally distinguish two gravitational-wave signals, and hence the models that generate them. The systematic errors generated by different models of nuclear reactions raise questions somewhat different from that of comparing different matter equations of state. We need to ask if different physics implementations for the *same* equation of state can be observationally distinguished. This question motivates the present work.

Here we focus on the impact of nuclear reactions on the gravitational-wave signal recovered from simulations. In the simplest case, the reactions are responsible for the balance between neutrons, protons, and electrons in the high-density matter and are also responsible for production

---

[*]Corresponding author.
p.c.hammond@soton.ac.uk

of neutrinos in neutron stars (which, in turn, leads to bulk viscosity [17]). While there are current efforts [15,18–21] to include neutrinos in neutron-star merger simulations, we are only aiming to get a handle on the "error bars" involved, so we take a more simplistic approach. We consider two limiting cases, such that the reactions either take place on such a long timescale that the rates can be set to zero, or on such a short timescale that the fluid composition reaches equilibrium instantaneously. As a proof of principle, we use a single equation of state for our simulations to isolate the systematic errors due to the model for nuclear reactions. We then use toy models to motivate the robustness of our results to changes in other aspects of the model, such as the stiffness of the equation of state. Our results demonstrate that gravitational-wave signals from these two simulations—although very similar—could be distinguishable with a third-generation instrument like the Einstein Telescope or Cosmic Explorer. The implications are simple. We either have to accept the difference as a systematic error or we need to make progress on implementing nuclear reactions in our simulations.

II. METHOD

A. Simulating reaction limits

We assume the neutron-star fluid is composed of neutrons, protons, and electrons, which have number densities n_n, n_p, and n_e, respectively, and that the fluid is locally charge neutral, which imposes the condition $n_p = n_e$. We then define the baryon number density as $n_b = n_n + n_p$, proportional to the fluid rest mass density ρ. To keep track of the composition of the fluid, we use the electron fraction Y_e defined by

$$Y_e = \frac{n_e}{n_b} = \frac{n_p}{n_b}. \tag{1}$$

The standard Valencia formulation [22,23] of the general relativistic evolution equations already accounts for the evolution of n_b through ρ, however, an extra equation is required for the evolution of Y_e. This takes the form

$$u^a \nabla_a Y_e = \frac{\Gamma_e}{n_b}, \tag{2}$$

where u^a is the fluid four velocity, and Γ_e is the total rate of electron production (for the simplest case of the Urca processes, this will be the rate of neutron decay minus the rate of electron capture). The left-hand side of the equation accounts for the advection of the composition along the world line of a given fluid element, and the right-hand side accounts for the change in this composition due to reactions.

While this relation is simple to write down, the interaction between the rates and the numerical methods make it much less simple to evolve. If the reaction rate Γ_e is large

compared to $n_e \Delta t$ (where Δt is the simulation time step), or equivalently, the equilibration timescale of the reactions is fast compared to Δt, then Eq. (2) becomes stiff and explicit numerical evolution schemes produce unphysical oscillations in Y_e. The standard workarounds for this (decrease Δt, increase convergence order, use an implicit scheme,[1] etc.) are either computationally expensive or would require significant changes to the method used (or both), so as a first step we instead work in the two limits of Γ_e: the fast-reaction limit where $\Gamma_e \to \infty$ and the slow-reaction limit where $\Gamma_e \to 0$.

In the slow-reaction limit, Eq. (2) simplifies to a standard advection equation where fluid composition is preserved along the world lines of fluid elements, while the assumption that the reactions occur on timescales too fast to be resolved by the simulation will cause the matter to always be in β equilibrium. The definition of this equilibrium (in terms of chemical potentials) changes as the temperature of the fluid varies due to different reactions dominating the changes in composition [11,25]. As we are not yet able to implement this effect—we do not have access to the extra chemical potentials required for the other equilibria [25]—we bypass the issue by using (for the fast-limit simulation) the "cold" β equilibrium, $\mu_n = \mu_p + \mu_e$. While reality may lie closer to one of these limits than the other, the estimates given in [11,17] indicate that it is difficult to judge which limit would be the more accurate when applied to *all* of the matter. A full transport scheme would be required to determine whether either limit is appropriate, and, on the way to such a simulation, investigating these two limits is a natural first step.

We describe our current simulation setup in detail in [11]. Briefly, we use a standard set of thorns within the Einstein Toolkit [26] modified to facilitate the use of three-parameter tabulated equations of state; in particular, we use the Akmal-Pandharipande-Ravenhall [27,28] equation of state. The simulation uses adaptive mesh refinement for the grid, with the highest spacial resolution grids being centered on and completely covering each star with a grid spacing of ~ 400 m, and the time step we use is $\Delta t/\Delta x = 0.25$. A single set of initial data for two stars, each with baryon mass $M_b = 1.4 M_\odot$, separated by 40 km obtained using LORENE [29], is evolved in all simulations presented here, assuming a fixed initial temperature of $T = 0.02$ MeV and cold β equilibrium. No magnetic fields are present.

In order to keep the simulations as comparable as possible, we use identical code for the in- and out-of-equilibrium simulations, and account for the instantaneous equilibration through the equation of state table. In order to

---

[1]This is the approach used by Most *et al.* [24], however, the accuracy of implicit schemes in regions where an explicit scheme would not otherwise be stable is questionable. This issue needs further consideration.

achieve this, we take the 2D slice defined by $\mu_{\mathrm{n}} = \mu_{\mathrm{p}} + \mu_{\mathrm{e}}$ through the full three-parameter table, then replace each value of $p(\rho, T, Y_{\mathrm{e}})$ in the three-parameter table with the value $p(\rho, T)$ found on the 2D slice (and equivalently for other equation of state variables). We can then use this table with the same interface as the original table.

B. Gravitational-wave analysis

We measure the gravitational radiation from the merger through the Weyl scalar $\Psi_4 = \ddot{h}_+ - i\ddot{h}_\times$, using the "fixed frequency integration" method of Reisswig and Pollney [30] to obtain the raw strain $h = h_+ - ih_\times$. As the stars remain close to equilibrium until merger, we do not expect any significant differences to appear during the inspiral (and indeed we do not see significant differences between the simulations in the ~ 5 premerger orbits covered), hence we focus our analysis on the postmerger signal. We do this in two ways: in one method, we ignore any data before the maximum $|h(t)|$; in the second, we apply a high-pass filter to all of the data.

To quantify the impact of the reaction limits on the recovered signals, we use a standard measure of the difference between two gravitational-wave signals, the mismatch $\mathcal{M}$ (see, e.g., [31–34]). The mismatch is calculated through the waveform overlap $\langle h_1 | h_2 \rangle$, defined by

$$\langle h_1 | h_2 \rangle = 4 \int_{-\infty}^{\infty} \frac{\tilde{h}_1(f)\tilde{h}_2^*(f)}{S_n(f)} \, \mathrm{d}f, \qquad (3)$$

where $\hat{h}(f)$ is the Fourier transform of h and $*$ denotes its complex conjugate, while S_n is the strain sensitivity of a detector as power spectral density. As the simulation outputs a discretely sampled signal, we discretize Eq. (3) to obtain

$$\langle h_1 | h_2 \rangle = 4\Delta f \sum_{f=f_{\min}}^{f_{\max}} \left(\frac{\tilde{h}_1(f)\tilde{h}_2^*(f)}{S_n(f)} \right), \qquad (4)$$

where the tilde denotes the discrete Fourier transform (normalized for consistency with the continuous version), $f_{\max}$ is the maximum resolvable frequency in the data (typically the Nyquist frequency), $f_{\min}$ is the minimum resolvable frequency (which for us is either the fixed cutoff frequency ω_0 used in the fixed frequency integration [30] or the filter frequency), and Δf is the frequency resolution of the discrete Fourier transform.

The match M (sometimes referred to as the "maximized overlap") between the two signals is given by

$$\mathrm{M} = \frac{\max(\langle h_1 | h_2 \rangle)}{\sqrt{\langle h_1 | h_1 \rangle \langle h_2 | h_2 \rangle}}, \qquad (5)$$

where the overlap between h_1 and h_2 should be maximized by time and phase shifting h_2 by (t_c, ϕ_c). The mismatch $\mathcal{M}$ is then given by one minus the real part of the (maximized) match, so we obtain

$$\mathcal{M} = 1 - \Re \left(\frac{\max(\langle h_1 | h_2 e^{i(\phi_c - 2\pi f t_c)} \rangle)}{\sqrt{\langle h_1 | h_1 \rangle \langle h_2 | h_2 \rangle}} \right). \qquad (6)$$

The mismatch is related to the signal-to-noise ratio of the difference between the two signals ρ_{diff} through [32]

$$\rho_{\mathrm{diff}}^2 = 2\rho_{\mathrm{sig}}^2 \mathcal{M}, \qquad (7)$$

where ρ_{sig} is the signal-to-noise ratio of a detected signal (not to be confused with the matter density). A widely used criterion for the two signals to be distinguishable is $\rho_{\mathrm{diff}} \geq 1$ [31,35]. It should be noted that this does not relate to the ability to observe a signal among some noise, nor to using a given signal to estimate the specific model differences. Instead, it speaks to whether or not one is able distinguish between one model and another, knowing that there is a signal present in the data.

For our purposes, we want to know what signal-to-noise ratio is required for us to be able to distinguish between the two reaction limits, so we rearrange Eq. (7) to provide the condition

$$\rho_{\mathrm{sig}} \geq \frac{1}{\sqrt{2\mathcal{M}}}. \qquad (8)$$

To reiterate, if this condition is satisfied for a given detected signal, we should be able to differentiate between fast- and slow-reaction-limit behavior. We define $\rho_{\mathrm{req}} = 1/\sqrt{2\mathcal{M}}$ as the smallest signal-to-noise ratio required to satisfy this condition.

III. RESULTS AND DISCUSSION

A. Waveform comparison

In the upper panel of Fig. 1, we show the postmerger gravitational-wave output of the fast- and slow-reaction-limit simulations, alongside the suggested ET-D noise curve for the Einstein Telescope [5] (which we use as the detector noise in all mismatch calculations), assuming a polar aligned detector at a distance of 40 Mpc. While the two signals have similar overall shapes in the frequency domain, we see that the peak frequencies for the two simulations are visibly different: 2992 ± 8 Hz in the slow-limit simulation and 3050 ± 10 Hz in the fast-limit simulation, giving a difference of $\Delta f = 58 \pm 13$ Hz. Peak frequencies are calculated using the method of Macleod [36] and checked using the method of Quinn [37] (in all cases, the estimate from the second method is within the error bounds of the first). The computed mismatch between these signals is $\mathcal{M} = 36\%$, which, using Eq. (8), gives a required signal-to-noise ratio for the two signals to be distinguishable of $\rho_{\mathrm{req}} = 1.2$. As this is lower than any reasonable threshold to claim a detection, if the postmerger signal is detected, then the effect of the reactions must be taken into account.
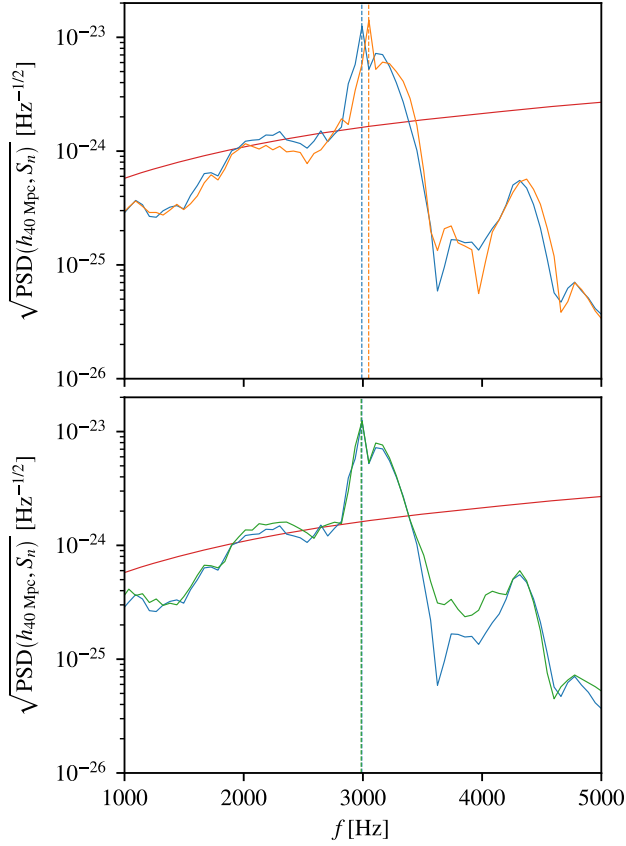
FIG. 1. Upper: square-root power spectral density (PSD) plots of the recovered waveforms from slow- and fast-reaction-limit simulations (blue and orange curves, respectively). Lower: the same comparison for the high- and low-resolution simulations (blue and green curves, respectively), both in the slow-reaction limit. Upper and lower: peak frequencies for each curve calculated using the Macleod method [36] are shown with dashed lines. The ET-D design sensitivity curve for the Einstein Telescope [5] is shown in red. The waveforms are normalized to a distance of 40 Mpc and assume the source and detector are perfectly aligned.

As a sanity check, we also performed a simulation with 20% coarser resolution but otherwise identical to the slow-limit simulation, the output of which is plotted (alongside the original slow-limit results) in the lower panel of Fig. 1. Comparing these results with the original slow-limit simulation, we find a mismatch on the order of 1%, and the lower resolution simulation has a measured peak frequency of 2992 ± 6 Hz. The mismatch in this case is much lower than the mismatch between the fast- and slow-limit simulations, and the peak frequency extracted from the low-resolution simulation is within the error bounds of the high-resolution simulation, so we are confident that the numerical error due to the finite resolution of the simulations is much less than the difference driven by the contrasting physics models in the two cases.

As a further check, we have performed the above analysis using the full gravitational-wave data from each simulation (as opposed to just the postmerger data) after high-pass filtering (the methodology used in [38]) and obtained mismatches of 33% and 1% for the fast-/slow-limit and high-/low-resolution combinations, respectively. All of the recovered peak frequencies were within the error bounds of their counterparts given above.

B. Effect on the equation of state

Having established that the two cases are distinguishable, it is natural to question what drives this difference. We start by using a simple model motivated by the results of the simulations to explore what effect being out of equilibrium has on an isolated star. By constructing two one-parameter equations of state from the full three-parameter table, one in- and one out-of-equilibrium, we can see what effect being out of equilibrium has on the structure of the stars. For the out-of-equilibrium equation of state, we solve the composition for a constant $\mu_\Delta = \mu_n - (\mu_p + \mu_e)$ throughout the table. This value of the offset need not be wholly representative of the full simulations, but for the sake of comparison we use the simulation data to inform our choice. In Figs. 5 and 7 of [11], we see the deviation from chemical equilibrium in the two stars around the time of merger. At 5 ms postmerger, most of the core matter is in the $\mu_\Delta = 20$–30 MeV range (excluding the hot spots), hence we choose $\mu_\Delta = 20$ MeV as the deviation from equilibrium for our out-of-equilibrium equation of state. Finally, we obtain a one-parameter equation of state by choosing a temperature of $T = 5$ MeV.

Using LORENE [29], we first construct a rotating star using the equilibrium equation of state. We choose the mass of the star such that the central baryon number density is similar to that found in our simulation ($3.5n_{\mathrm{sat}}$), giving a total baryon mass for the star of $1.7M_\odot$, and an arbitrary rotation frequency of 500 Hz (significant, but well below the Keplerian frequency). This gives us a total angular momentum. We then construct a rotating star using the out-of-equilibrium equation of state conserving the total baryon mass and angular momentum from the equilibrium star, giving us a different rotation frequency. Admittedly, this toy model is far from the true, dynamical postmerger state. However, its qualitative features (in terms of rotation rates and hence gravitational-wave phasing) should match a full model and allow us to robustly explore a range of equations of state.

We find that, to conserve angular momentum, the rotation frequency must be reduced to 496 Hz (a fractional difference of ~1%). We repeated this procedure for a number of equations of state based on different physical models, namely, the DD2 [39,40], SFHx [41], and SLy4 [42,43] equations of state, and obtained similar results, with the change in rotation frequency required being of order 1% and always in the same direction: out-of-equilibrium stars need a lower frequency to match the angular momentum of the respective in-equilibrium stars due to an increase in moment

of inertia. This increase is caused by a softening of the equation of state at core densities as the matter is taken out of equilibrium, creating a flatter density profile, and thus more of the mass of the star is located further from the axis of rotation.

Having observed similar effects in several equations of state, one might ask whether this effect is truly general. We will do this through the adiabatic index

$$\Gamma = \left.\frac{\partial \ln p}{\partial \ln n_b}\right|_{\mathcal{S},Y_e} = \frac{n_b}{p}\left.\frac{\partial p}{\partial n_b}\right|_{\mathcal{S},Y_e}, \tag{9}$$

where $\mathcal{S}$ is the specific entropy per baryon. Taylor expanding around equilibrium and keeping only the first term, we obtain

$$\Gamma(\mu_\Delta) = \Gamma(0) + \mu_\Delta \left.\frac{\partial \Gamma(0)}{\partial \mu_\Delta}\right|_{\mathcal{S},n_b} + \mathcal{O}(\mu_\Delta^2), \tag{10}$$

so the change in stiffness when moving out of equilibrium will depend on the sign of the second term. The sign is dependent on the equation of state used, however, assuming a simple Fermi gas model gives a negative value for all densities. Using the more realistic BSk density functionals [44] we also obtain a negative sign at the densities of interest.

C. Effect on the matter distribution

Having examined some simpler systems to determine a possible source for the frequency difference presented above, we can also look to see whether the softening effect is visible in the full merger simulation. The naïve approach would be to measure the moment of inertia of the whole system in each case. However, after merger, the moment of inertia is dominated by low-density matter far from the remnant, so we need some local measure that we can apply only to the remnant.

Starting from the Newtonian definition of the moment of inertia for a mass distribution along the z axis,

$$I_z(\rho) = \iiint_V \rho(x,y,z)(x^2+y^2)\mathrm{d}V, \tag{11}$$

we substitute in the proper mass density ρW (the rest mass density ρ multiplied by the local Lorentz factor W), and correct the volume element to obtain

$$I^z = \iiint_V \rho W(x^1 x^1 + x^2 x^2)\sqrt{\gamma}\mathrm{d}^3 x. \tag{12}$$

To better see the differences between the remnants, we will use a density cutoff to mask the effects of low-density matter at large radius, and to determine a relevant density for the cutoff, we will look at how the contribution to the
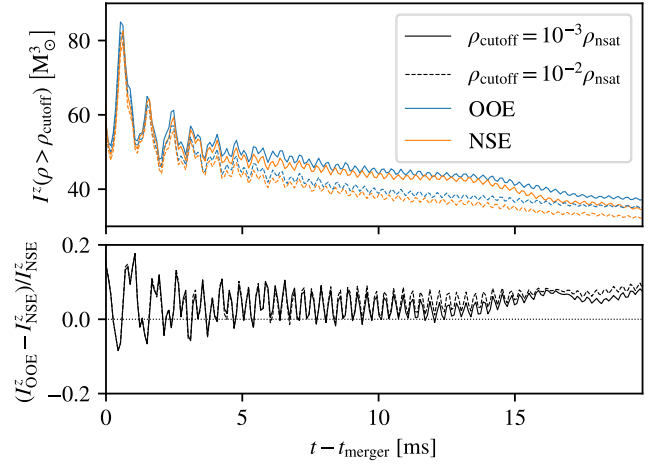

FIG. 2. Upper: evolution of the total moment of inertia [see Eq. (12)] ignoring matter with rest mass density below ρ_{cutoff} for slow- and fast-reaction-limit simulations (labeled OOE for out of equilibrium and NSE for in equilibrium, solid and dotted lines, respectively). Lower: relative difference between results for slow- and fast-limit simulations.

moment of inertia varies in the x-y plane of the two stars. To do this, we calculate the infinitesimal contribution to the total moment of inertia of the loop at radius r, $I^{\text{loop}}(r)$, then integrate radially outward [to obtain $I^{\text{disk}}(r)$] to find the density at which the difference between the two simulations settles to a particular value. We find that the difference between $I^{\text{disk}}_{\text{OOE}}$ and $I^{\text{disk}}_{\text{NSE}}$ reaches a near steady state by $\rho \sim 10^{-2} - 10^{-3}\rho_{\text{sat}}$.

Ignoring densities below this cutoff, we can then apply Eq. (12) to the whole domain, the results of which we plot in Fig. 2. This shows that, when considering only the densities above $\rho_{\text{cutoff}} \sim 10^{-2} - 10^{-3}\rho_{\text{sat}}$, the moment of inertia of the remnant is a few percent higher in the out-of-equilibrium simulation, which would intuitively lead to a few percent decrease in the frequency at which the remnant rotates.

IV. SUMMARY

We have shown that the *postmerger* gravitational-wave signal is sensitive to the model of the weak reactions, in concordance with recent simulations, using a different method, by Most *et al.* [24]. This is driven by an increase in moment of inertia from softening of the equation of state which, we argue, is robust across different equation of state models. If the bulk equation of state is constrained by the inspiral and merger phase of the signal [45], then this dephasing from the fixed equation of state model would be distinguishable with the next-generation gravitational-wave observatories, like the Einstein Telescope and Cosmic Explorer.

It is, of course, important to note that the change in frequency seen here is, in general, small compared to the

difference in frequency obtained by changing the equation of state (see, for example, Takami *et al.* [38]). However, we reiterate that the magnitude of the deviation demonstrated here is enough to materially alter the postmerger gravitational-wave spectrum as would be seen by a generation detector. Therefore, any parameters extracted from such a signal using templates derived from simulations that do not take this effect into account would be subject to an associated systematic error. If we wish to maximize the science output of the next generation of detectors, consistent models of weak reactions and numerical simulations including them are essential.

[1] B. P. Abbott *et al.*, GW170817: Observation of Gravitational Waves from a Binary Neutron Star Inspiral, Phys. Rev. Lett. **119**, 161101 (2017).

[2] L. Baiotti and L. Rezzolla, Binary neutron star mergers: A review of Einstein's richest laboratory, Rep. Prog. Phys. **80**, 096901 (2017).

[3] S. Bernuzzi, Neutron star merger remnants, Gen. Relativ. Gravit. **52**, 108 (2020).

[4] M. Punturo *et al.*, The Einstein Telescope: A third-generation gravitational wave observatory, Classical Quantum Gravity **27**, 194002 (2010).

[5] S. Hild *et al.*, Sensitivity studies for third-generation gravitational wave observatories, Classical Quantum Gravity **28**, 094013 (2011).

[6] The Einstein Telescope, http://www.et-gw.eu/.

[7] D. Reitze *et al.*, Cosmic explorer: The U.S. contribution to gravitational-wave astronomy beyond LIGO, Bull. Am. Astron. Soc. **51**, 035 (2019), https://baas.aas.org/pub/2020n 7i035.

[8] Cosmic Explorer, https://cosmicexplorer.org/.

[9] L. Baiotti, Gravitational waves from binary neutron stars, Arabian J. Math. **9**, 105 (2022).

[10] T. Dietrich, D. Radice, S. Bernuzzi, F. Zappa, A. Perego, B. Brügmann, S. V. Chaurasia, R. Dudi, W. Tichy, and M. Ujevic, CoRe database of binary neutron star merger waveforms, Classical Quantum Gravity **35**, 24LT01 (2018).

[11] P. Hammond, I. Hawke, and N. Andersson, Thermal aspects of neutron star mergers, Phys. Rev. D **104**, 103006 (2021).

[12] R. M. Cabezón, K.-C. Pan, M. Liebendörfer, T. Kuroda, K. Ebinger, O. Heinimann, A. Perego, and F.-K. Thielemann, Core-collapse supernovae in the hall of mirrors, Astron. Astrophys. **619**, A118 (2018).

[13] K.-C. Pan, C. Mattes, E. P. O'Connor, S. M. Couch, A. Perego, and A. Arcones, The impact of different neutrino transport methods on multidimensional core-collapse supernova simulations, J. Phys. G **46**, 014001 (2018).

[14] S. Richers, H. Nagakura, C. D. Ott, J. Dolence, K. Sumiyoshi, and S. Yamada, A detailed comparison of multidimensional boltzmann neutrino transport methods in core-collapse supernovae, Astrophys. J. **847**, 133 (2017).

[15] M. Cusinato, F. M. Guercilena, A. Perego, D. Logoteta, D. Radice, S. Bernuzzi, and S. Ansoldi, Neutrino emission from binary neutron star mergers: Characterizing light curves and mean energies, Eur. Phys. J. A **58**, 99 (2022).

[16] A. Mezzacappa, E. Endeve, O. E. B. Messer, and S. W. Bruenn, Physical, numerical, and computational challenges of modeling neutrino transport in core-collapse supernovae, Living Rev. Comput. Astrophys. **6**, 4 (2020).

[17] T. Celora, I. Hawke, P. C. Hammond, N. Andersson, and G. L. Comer, Formulating bulk viscosity for neutron star simulations, Phys. Rev. D **105**, 103016 (2022).

[18] D. Radice, S. Bernuzzi, A. Perego, and R. Haas, A new moment-based general-relativistic neutrino-radiation transport code: Methods and first applications to neutron star mergers, Mon. Not. R. Astron. Soc. **512**, 1499 (2022).

[19] A. Camilletti, L. Chiesa, G. Ricigliano, A. Perego, L. C. Lippold, S. Padamata, S. Bernuzzi, D. Radice, D. Logoteta, and F. M. Guercilena, Numerical relativity simulations of the neutron star merger GW190425: Microphysics and mass ratio effects, Mon. Not. R. Astron. Soc. **516**, 4760 (2022).

[20] C. Palenzuela, S. L. Liebling, and B. Miñano, Large eddy simulations of magnetized mergers of neutron stars with neutrinos, Phys. Rev. D **105**, 103020 (2022).

[21] K. Hayashi, S. Fujibayashi, K. Kiuchi, K. Kyutoku, Y. Sekiguchi, and M. Shibata, General-relativistic neutrino-radiation magnetohydrodynamics simulation of black hole-neutron star mergers for seconds, Phys. Rev. D **106**, 023008 (2022).

[22] F. Banyuls, J. A. Font, J. M. Ibanez, J. M. Marti, and J. A. Miralles, Numerical $\{3+1\}$ general relativistic hydrodynamics: A local characteristic approach, Astrophys. J. **476**, 221 (1997).

[23] L. Baiotti, I. Hawke, P. J. Montero, F. Löffler, L. Rezzolla, N. Stergioulas, J. A. Font, and E. Seidel, Three-dimensional relativistic simulations of rotating neutron star collapse to a Kerr black hole, Phys. Rev. D **71**, 024035 (2005).

[24] E. R. Most, A. Haber, S. P. Harris, Z. Zhang, M. G. Alford, and J. Noronha, Emergence of microphysical viscosity in binary neutron star post-merger dynamics, arXiv:2207.00442.

[25] M. G. Alford and S. P. Harris, β equilibrium in neutron-star mergers, Phys. Rev. C **98**, 065806 (2018).

[26] Z. Etienne *et al.*, The Einstein Toolkit (accessed 2021), http://einsteintoolkit.org/index.html.

[27] A. Akmal, V. R. Pandharipande, and D. G. Ravenhall, Equation of state of nucleon matter and neutron star structure, Phys. Rev. C **58**, 1804 (1998).

[28] A. S. Schneider, C. Constantinou, B. Muccioli, and M. Prakash, Akmal-Pandharipande-Ravenhall equation of state for simulations of supernovae, neutron stars, and binary mergers, Phys. Rev. C **100**, 025803 (2019).

[29] E. Gourgoulhon, P. Grandclément, and J. Novak, LORENE (accessed 2022), https://lorene.obspm.fr/.

[30] C. Reisswig and D. Pollney, Notes on the integration of numerical relativity waveforms, Classical Quantum Gravity **28**, 195015 (2011).

[31] L. Lindblom, B. J. Owen, and D. A. Brown, Model waveform accuracy standards for gravitational wave data analysis, Phys. Rev. D **78**, 124020 (2008).

[32] S. T. McWilliams, B. J. Kelly, and J. G. Baker, Observing mergers of nonspinning black-hole binaries, Phys. Rev. D **82**, 024014 (2010).

[33] E. Baird, S. Fairhurst, M. Hannam, and P. Murphy, Degeneracy between mass and spin in black-hole-binary waveforms, Phys. Rev. D **87**, 024035 (2013).

[34] P. Kumar, K. Barkett, S. Bhagwat, N. Afshari, D. A. Brown, G. Lovelace, M. A. Scheel, and B. Szilágyi, Accuracy and precision of gravitational-wave models of inspiraling neutron star-black hole binaries with spin: Comparison with matter-free numerical relativity in the low-frequency regime, Phys. Rev. D **92**, 102001 (2015).

[35] M. Pürrer and C.-J. Haster, Gravitational waveform accuracy requirements for future ground-based detectors, Phys. Rev. Res. **2**, 023151 (2020).

[36] M. Macleod, Fast nearly ML estimation of the parameters of real or complex single tones or resolved multiple tones, IEEE Trans. Signal Process. **46**, 141 (1998).

[37] B. Quinn, Estimation of frequency, amplitude, and phase from the DFT of a time series, IEEE Trans. Signal Process. **45**, 814 (1997).

[38] K. Takami, L. Rezzolla, and L. Baiotti, Spectral properties of the post-merger gravitational-wave signal from binary neutron stars, Phys. Rev. D **91**, 064001 (2015).

[39] M. Hempel and J. Schaffner-Bielich, A statistical model for a complete supernova equation of state, Nucl. Phys. **A837**, 210 (2010).

[40] S. Typel, G. Röpke, T. Klähn, D. Blaschke, and H. H. Wolter, Composition and thermodynamics of nuclear matter with light clusters, Phys. Rev. C **81**, 015803 (2010).

[41] A. W. Steiner, M. Hempel, and T. Fischer, Core-collapse supernova equations of state based on neutron star observations, Astrophys. J. **774**, 17 (2013).

[42] A. S. Schneider, L. F. Roberts, and C. D. Ott, Open-source nuclear equation of state framework based on the liquid-drop model with Skyrme interaction, Phys. Rev. C **96**, 065802 (2017).

[43] E. Chabanat, P. Bonche, P. Haensel, J. Meyer, and R. Schaeffer, A Skyrme parametrization from subnuclear to neutron star densities Part II. Nuclei far from stabilities, Nucl. Phys. **A635**, 231 (1998).

[44] S. Goriely, N. Chamel, and J. M. Pearson, Further explorations of Skyrme-Hartree-Fock-Bogoliubov mass formulas. XIII. The 2012 atomic mass evaluation and the symmetry coefficient, Phys. Rev. C **88**, 024308 (2013).

[45] B. P. Abbott et al., GW170817: Measurements of Neutron Star Radii and Equation of State, Phys. Rev. Lett. **121**, 161101 (2018).

[46] P. Hammond, Source, parfile, and plotting scripts relating to "Thermal aspects of neutron star mergers", Zenodo, 10.5281/zenodo.5469497 (2021).

[47] P. Hammond, Parfile, and plotting scripts relating to "Detecting the impact of nuclear reactions on neutron star mergers through gravitational waves", Zenodo, 10.5281/zenodo.6532867 (2022).